A degenerate bifurcation to chaotic scattering in a multicentre potential

1995 J. Phys. A: Math. Gen. 28 6887

(http://iopscience.iop.org/0305-4470/28/23/029)

J. Phys. A: Math. Gen. 28 (1995) 6887–6902. Printed in the UK

A degenerate bifurcation to chaotic scattering in a multicentre potential

C Lipp† and C Jung‡

† Institut für Theoretische Physik, Universität Basel Klingelbergstrasse 82, CH-4056 Basel, Switzerland

‡ Instituto de Física, Laboratorio de Cuernavaca, UNAM Apartado Postal 139-B, 62191 Cuernavaca, Morelos, Mexico

Received 1 May 1995

Abstract. Many scattering systems can be described as scattering of a point particle off a multicentre potential. In this paper we present a two-centre system which shows either regular or chaotic scattering depending on the kinetic energy, i.e. the velocity of the incoming particle. The transition points to chaotic scattering can be derived analytically by linearization of the Poincaré map. At one of these transition velocities there is a degenerate bifurcation where the invariant set contains a parabolic surface and where the time delay statistics is algebraic with power $\sigma = 2$.

1. Introduction

The properties of a chaotic scattering system depend essentially on the values of the system parameters. For continuous potentials a natural parameter is the energy E and therefore in this paper we always study the scattering behaviour as a function of E or of some equivalent quantity. Of course, analogous results might be found as well for the dependence on completely different parameters.

A rather common scenario in scattering systems is the following: For $E > E_c$ the scattering is regular and there is no topological chaos in the energy surfaces F_E in phase space. For $E < E_c$ the scattering is chaotic and there is topological chaos in the energy surfaces. At $E = E_c$ a chaotic saddle Λ is created which causes the scattering functions as, for example, the deflection function or the time delay function to become chaotic, i.e. to show singularities on a fractal subset of their domain. For a recent overview of scattering chaos see the feature issue of the journal *Chaos* on chaotic scattering [1].

There exist two basically different generic bifurcation scenarios by which scattering can turn chaotic at $E = E_c$ [2]. In the first scenario the creation of Λ is initiated by a saddle-centre bifurcation of the most important periodic orbits. And for decreasing values of E more and more different periodic orbits are filled in by sequences of further saddle-centre bifurcations and by cascades of period doublings. Accordingly, the eigenvalues of the basic periodic orbits go to 1 for $E \to E_c$ from below and Λ is certainly not hyperbolic in a vicinity of E_c. Exactly at $E = E_c$, Λ consists of a single parabolic orbit. For a description of such an example, namely the scattering off the magnetic dipole, see [3].

In the second generic scenario Λ pinches to a line in the energy surface F_E for $E \to E_c$ from below while the eigenvalues of the periodic orbits go to infinity. Below E_c there is an energy interval (E_0, E_c) in which Λ is hyperbolic and structurally stable. For an early

0305-4470/95/236887+16$19.50

observation of such a case see [4]. Later this second scenario has been given the name 'abrupt bifurcation' [2, 5–6].

These two scenarios are the generic possibilities, how scattering can turn chaotic, but certainly they are not the only possibilities. To demonstrate the existence of further possibilities, in this paper we describe a degenerate case, in which Λ appears suddenly at $E = E_c$ in a scenario which has a mixture of features of the two scenarios mentioned above and so in addition some unusual properties. Namely, part of the periodic orbits becomes infinitely unstable and pinches to a line L_c while at the same time an elliptic fixed point together with its surrounding KAM island turns into a continuum of parabolic periodic orbits which for $E = E_c$ form a two-dimensional surface S_c within F_{E_c}. Part of L_c forms a part of the boundary line of S_c.

In section 2 we describe our particular model which is a two-centre Coulomb potential with hard cut-off. Section 3 contains the development of Λ as E approaches E_c from below and section 4 describes the unusual invariant set exactly at $E = E_c$. Section 5 shows an approach to the critical energy E_c in terms of a sequence of symbolic dynamics. In the final section we compare our model with some other situations and give some remarks why the study of it may be interesting even though it is a non-generic degenerate case.

2. The model

Let us consider the scattering of a point particle under the influence of two attractive cut off Coulomb potentials in a plane. The Hamiltonian is given by

$$H = p^2/2 + V(r_1) + V(r_2) \tag{1}$$

where r_1 and r_2 are the distances to the centres and the potential $V(r)$ consists of a Coulomb potential with a sharp cut-off at $r = a$:

$$V(r) = \begin{cases} 1/a - 1/r & r < a \\ 0 & r \geqslant a. \end{cases} \tag{2}$$

The centres are placed at $x = 0$ and $y = \pm R$. The constant term $1/a$ is added to $V(r)$ in order to avoid a discontinuity in the potential at $r = a$ and $2R$, the distance between the centres, is taken to be larger than $2a$, so there is no overlap of the two Coulomb potentials.

When we use the velocity v as a parameter in the following, then this always means the particle velocity outside of the potentials. Therefore it is equivalent to the total energy $E = v^2/2$ taken as parameter.

2.1. Scattering at one centre

The deflection function for the scattering at one of the potentials V only depends on the impact parameter b_{loc} with respect to the centre of the potential and on the energy, i.e. the velocity v of the particle in the asymptotic region. Outside the interaction region $r < a$ the motion of the particle is a straight line and inside each potential it can be described as a segment of a Kepler ellipse

$$\cos\varphi = \frac{L^2/r - 1}{\sqrt{2E_k L^2 + 1}} \tag{3}$$

with Kepler energy $E_k = v^2/2 - 1/a$ and angular momentum $L = b_{loc}v$.

For positive impact parameters the scattering angle can be written as

$$\theta(b_{\rm loc}, v) = 2\left(\arccos\frac{b_{\rm loc}^2 v^2 - a}{\sqrt{a^2 + a^2 b_{\rm loc}^2 v^4 - 2ab_{\rm loc}^2 v^2}} - \arccos\frac{b_{\rm loc}}{a}\right). \tag{4}$$

The first term results from the angle of the Kepler ellipse between the point where the particles enter the potential and the perihelion of the ellipse.

For negative impact parameters $\theta(b_{\rm loc}, v) = 2\pi - \theta(|b_{\rm loc}|, v)$.

If $b > a$ the particle does not reach the interaction region and therefore $\theta(b_{\rm loc}, v)$ is set to zero.

It is easy to see that $\theta(b_{\rm loc}, v) = \pi$ for $b_{\rm loc} = 0$ independent of the velocity. For later considerations it is essential that for $v = v_{\rm A} = a^{-1/2}$ the scattering angle also takes the value π for all values of $b_{\rm loc}$ in the interval $[-a, a]$. This can be seen by an elementary geometrical construction. In a Coulomb potential any Kepler ellipse to this particular energy is intersected by the cut-off circle of radius a in the two middle points of the flat sides, i.e. in the two points where the curvature is minimal. The tangent lines to these two points of the ellipse are parallel to each other.

For $v < v_{\rm A}$ the scattering angle is a monotonically increasing function of $b_{\rm loc}$ and for $v > v_{\rm A}$ it is monotonically decreasing. The one-centre system is integrable because the angular momentum L with respect to its centre is a conserved quantity.

2.2. *Scattering at two centres*

With two centres the angular momentum is no longer conserved and we may have chaotic scattering. A necessary [1] (but not sufficient [7]) condition for this is an infinite number of unstable localized orbits. Therefore let us have a look at the most important periodic orbits of our system along which the particle switches between the two Coulomb centres. There are three orbits of period one in the Poincaré map to be defined below (see figure 1):

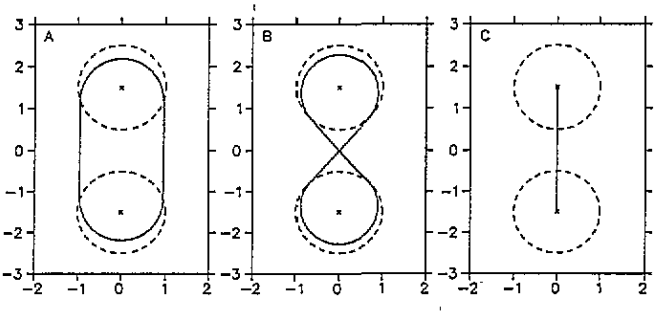

Figure 1. The three basic periodic orbits. The stadium A only occurs at $v = v_{\rm A}$, the figure-of-eight orbit B in the interval $v_{\rm B} < v < v_{\rm A}$ and the bouncing ball C at every velocity. The centres of the potentials are marked by crosses, the cut-off circles are plotted with broken curves.

(A) The stadium orbit where the particle runs parallel to the y-axis between the two potentials and always gets deflected at an angle of π. This orbit exists at the velocity $v_{\rm A} = a^{-1/2}$ for all impact parameters with absolute value less than a.

(B) The figure-of-eight orbit where the particle crosses the origin of our coordinate system after each deflection. The angle between the straight pieces of the trajectory depends on v and for each velocity in an interval $v_{\rm B} < v < v_{\rm A}$ there is exactly one orbit of this

type and its mirror image with reversed orientation. The value of the bifurcation velocity v_B will be derived in the next section.

(C) In the third simple periodic orbit the particle bounces directly between the centres of the two potentials and is always reflected at an angle of π. This bouncing ball orbit can be found at every velocity and it will become very important for understanding the overall development of Λ.

There are also two orbits of period two, one of which will be important later (see figure 2). They branch out of the orbit C at the velocity $v_C = (v_A + v_B)/2$ where the winding number of C (which will be defined in the next section) equals 1/2 and they exist in the interval $v_C < v < v_A$:

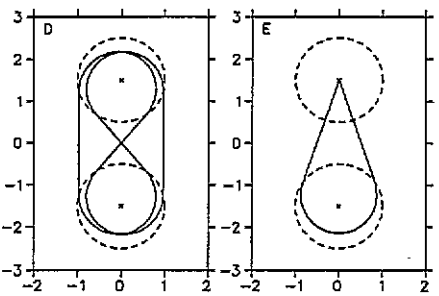

Figure 2. The two orbits of period two: the folded double loop D and the droplet orbit E. They both exist in an interval $v_C < v < v_A$.

(D) The folded double loop which can be overshadowed by segments of the stadium orbit and the figure-of-eight orbit alternatingly. Its symmetry partner runs along the same trace in position space with reversed orientation.

(E) The droplet orbit which runs directly into the upper centre under an angle $\gamma(v)$, is backscattered by π and then deflected by the lower potential region in such a way that it runs straight into the upper centre again with an angle of $-\gamma(v)$ where it bounces back again. The symmetry partner of this orbit can be obtained by a reflection in the x-axis.

Depending on the velocity there are many more periodic orbits which can all be overshadowed quite well by a few basic orbit segments along the following scheme. Cut any localized orbit into segments separated at the points where it crosses the y-axis at either $y > R$ or at $y < -R$. If the x component of the velocity has different signs at the initial and final point of a segment, then this segment is of similar qualitative structure as half a stadium orbit and we overshadow it by half a stadium orbit. If these two signs are the same, then this segment has a structure qualitatively similar to half of a figure-of-eight orbit and it is overshadowed by half this periodic orbit. As a further degenerate orbit element for overshadowing we introduce a piece of trajectory hitting directly a potential centre and being reflected in itself. By these three basic elements and all its mirror images about the symmetry lines of the potential we can overshadow any localized orbit and in particular any periodic orbit of the system.

The stadium orbit itself only exists at exactly $v = v_A$. Therefore for $v < v_A$ only finite blocks of the stadium type are allowed in the overshadowing process. For increasing v the maximally allowed length of these blocks increases and for $v \to v_A$ this maximal length converges to infinity giving the stadium orbit itself.

For all numerical examples shown in the rest of the paper we make the choice: $a = 1$, $R = 3/2$. This leads to $v_A = 1$.

3. Bifurcation scenario

In configuration space the centres of our potentials are located on the y-axis and symmetrically to the x-axis, so all trajectories have to cross the x-axis in order to switch between the two Coulomb centres. Therefore we take our Poincaré surface of section at $y = 0$ and $p_y > 0$. For any fixed value of the energy we take as coordinates in the two-dimensional plane of intersection b and γ, where b is the impact parameter with respect to the origin of our coordinate system and $\gamma = \arctan(p_x/p_y)$ is the angle between the velocity vector and the y-axis, $\gamma \in [-\pi/2, \pi/2]$.

The mapping M which describes the interaction of the particle with one of the centres is defined by

$$\gamma' = \gamma - \theta(b + R\sin\gamma, v) \tag{5}$$

$$b' = b + R\sin\gamma + R\sin\gamma'. \tag{6}$$

This map M can be interpreted as a symmetry reduced Poincaré map where we disregard the sign of p_y at the moment of intersection with the plane $y = 0$ and thereby we reduce out the reflection symmetry in the line $y = 0$. The Poincaré map itself is given by M^2. In figure 3 some plots of the section are shown for different velocities.

3.1. Linearization of the map

The linearization of M around a fixed point (b_0, γ_0) is given by

$$\tilde{M} = \begin{pmatrix} 1 - \theta' R\cos\gamma_0 & -\theta' \\ R\cos\gamma_0(2 - \theta' R\cos\gamma_0) & 1 - \theta' R\cos\gamma_0 \end{pmatrix} \tag{7}$$

where

$$\theta' = \left.\frac{\mathrm{d}\theta(b_{\mathrm{loc}}, v)}{\mathrm{d}b_{\mathrm{loc}}}\right|_{b_{\mathrm{loc}} = b_0 + R\sin\gamma_0}. \tag{8}$$

As noted before the bouncing ball orbit exists at every velocity thereby giving a persistent fixed point at (0,0) in our mappings. The eigenvalues of $\tilde{M}$ around this point are given by

$$\lambda_\pm = 1 - 2R(1/a - v^2) \pm 2R\sqrt{(1/a - v^2)(1/a - 1/R - v^2)} \tag{9}$$

and the bifurcation velocities where the eigenvalues change from real to complex are

$$v_{\mathrm{A}} = \sqrt{1/a} \qquad v_{\mathrm{B}} = \sqrt{1/a - 1/R}. \tag{10}$$

Introducing a new parameter d for the relative distance of the energy from the bifurcation points

$$d = (v_{\mathrm{A}}^2 - v^2)/(v_{\mathrm{A}}^2 - v_{\mathrm{B}}^2) = R(1/a - v^2) \tag{11}$$

the eigenvalues can be rewritten as

$$\lambda_\pm = -(\sqrt{d} \pm \sqrt{d - 1})^2 \tag{12}$$

where $d = 1$ corresponds to $v = v_{\mathrm{B}}$ and $d = 0$ for $v = v_{\mathrm{A}}$. Because $\det\tilde{M} = 1$ we find $\lambda_+\lambda_- = 1$.

For velocities $v < v_{\mathrm{B}}$ where $d > 1$ we get negative eigenvalues in the map M but positive eigenvalues for M^2 and so the fixed point (0,0) is hyperbolic.

For $v_{\mathrm{B}} < v < v_{\mathrm{A}}$ the two eigenvalues are complex conjugates of each other with $|\lambda| = 1$ thus leading to an elliptic fixed point.

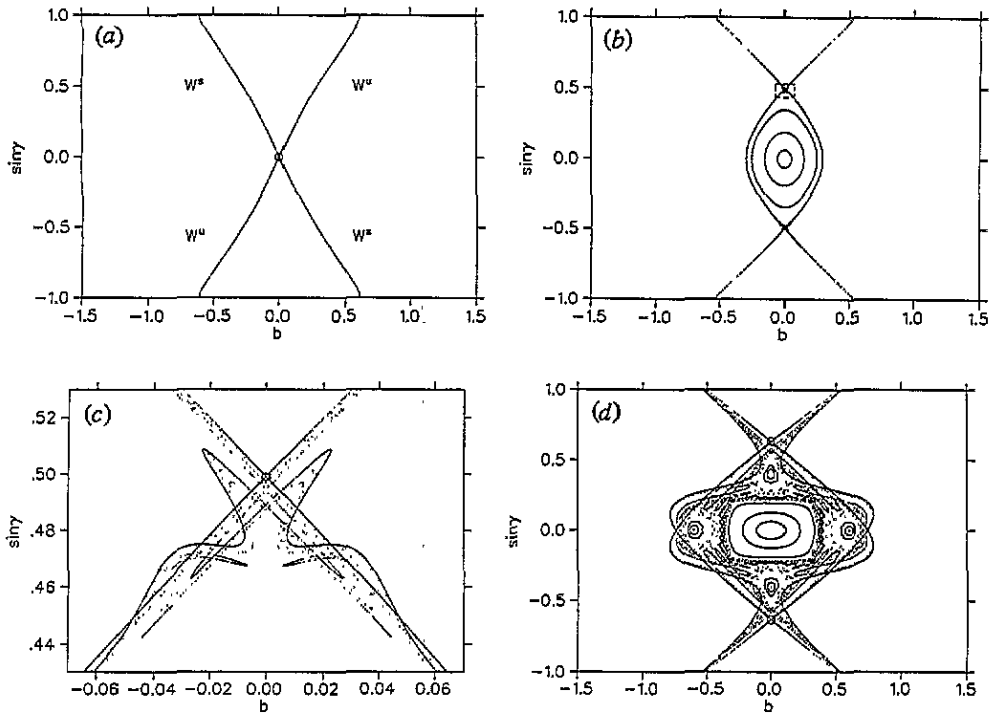

Figure 3. The Poincaré surface of section for various values of the velocity: (*a*) The invariant manifolds of the bouncing ball orbit C for $v = 0.5$. (*b*) The invariant manifolds of the figure eight orbit B and its symmetry partner for $v = 0.7$. Some KAM lines around the now stable bouncing ball orbit are also shown. (*c*) Magnification of the environment of one of the fixpoints as shown in (*b*) by broken curves. (*d*) The same as (*b*) for $v = 0.85$. In addition some KAM lines around the two different symmetry related folded double loops D of period 2 are shown. (*e*) The same as (*b*) for $v = 0.9$. (*f*) The same as (*b*) for $v = 0.965$. (*g*) The same as (*b*) for $v = 0.999$. (*h*) The same as (*a*) for $v = 1.01$. Open circles mark the position of unstable fixpoints.

For $v > v_A$ where d is negative the eigenvalues of M are positive and the fixed point is hyperbolic again.

Now let us consider the angle of the complex eigenvalue which is defined by

$$\delta = \arccos \frac{\operatorname{Re} \lambda}{|\lambda|} = \arccos(1 - 2d). \tag{13}$$

At each value of v where δ is a rational multiple of 2π there is a bifurcation leading to higher periodic points in our map M. For the Poincaré map M^2 we have to look at rational multiples of π. Therefore we define the winding number $w(v)$ as

$$w(v) = \frac{\delta}{\pi} = \frac{1}{\pi} \arccos(1 - 2R/a + 2Rv^2). \tag{14}$$

For $v = v_B$ the winding number equals 1 and with increasing velocity it becomes smaller until $w(v) = 0$ at $v = v_A$. At velocities where $w(v)$ is a rational number p/q we obtain orbits of period q branching out of the bouncing ball orbit. For example at $w(v) = 1/2$ the orbits D and E are created as stable und unstable counterparts (figure 2).

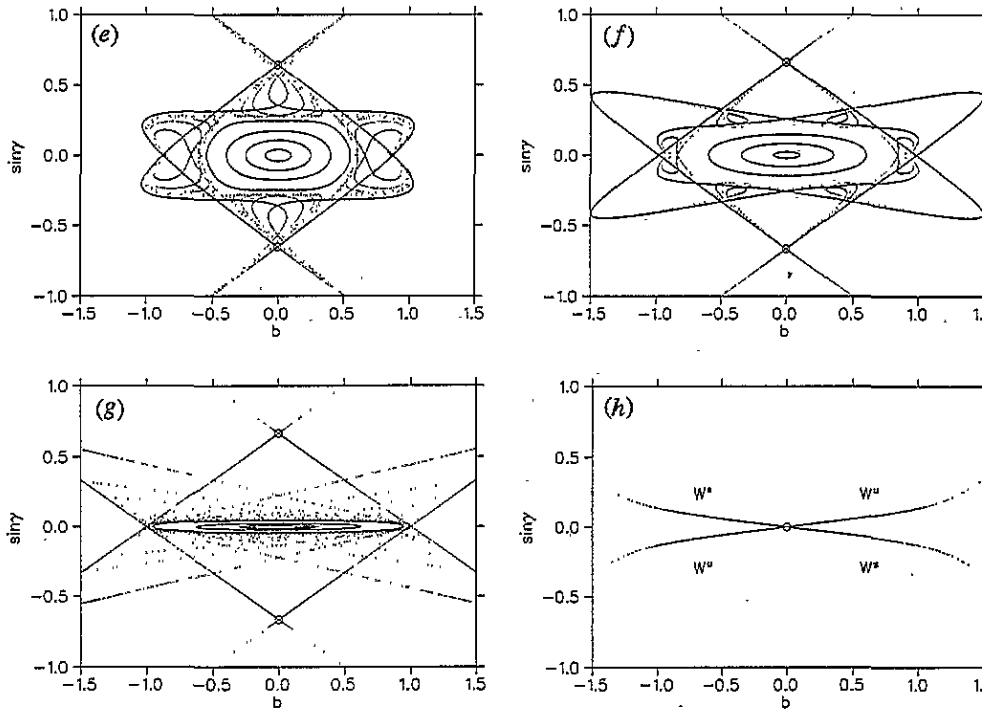

Figure 3. (Continued)

3.2. Scattering functions

As noted in the introduction chaotic scattering can be characterized by a fractal set of singularities in the scattering functions. These singularities occur at initial conditions where the particle gets arbitrarily close to one of the unstable localized orbits of the system.

When looking for the scattering functions in our model we fix the angle of the incoming particle and vary the impact parameter b. Our scattering functions are the number of bounces (passings through non-zero potential regions) and the scattering angle (outgoing angle) of the particle. At the singularities the number of bounces goes to infinity and the scattering angle is undefined which means it varies from $-\pi$ to π in any small interval including a singularity.

3.3. The development of Λ *with increasing energy*

With increasing energy or asymptotic velocity v the invariant set Λ develops as follows.

(i) For $v < v_B$ there is only one localized orbit (the bouncing ball orbit) which belongs to a hyperbolic fixed point at (0,0) in the Poincaré map. As figure 3(a) demonstrates, its invariant manifolds radiate into the asymptotic region directly without the creation of homoclinic intersections. Accordingly there is no chaotic invariant set (no chaotic saddle), the scattering functions as a function of the impact parameter have a few isolated singularities at worst and the scattering is regular.

(ii) For $v \to v_B$ from below the eigenvalues of the bouncing ball orbit converge towards 1 and the first bifurcation takes place at $v = v_B$ where $w(v) = 1$. For symmetry reasons it is a pitchfork bifurcation where the bouncing ball orbit itself becomes elliptic and branches

off two hyperbolic fixed points which belong to the figure-of-eight orbit B and its mirror image. Figure 3(*b*) shows the Poincaré section for a value of v just slightly above the bifurcation value v_B. As we can see in the magnification given in figure 3(*c*), the stable and unstable manifolds of these newly born unstable fixed points form homoclinic and heteroclinic intersections. Accordingly the Poincaré map contains a horseshoe construction leading to a chaotic invariant set. It is unstable, a so called chaotic saddle, and its fractal bundle of invariant manifolds radiates out into the asymptotic region making the scattering functions chaotic. Close to v_B the chaotic strips are extremely small and hard to detect in a Poincaré plot. With increasing v they become wider and chaos occupies a larger area in the plane of intersection.

(iii) Inside the interval $v \in (v_B, v_A)$ the winding number $w(v)$ of the elliptic fixed point at (0,0) monotonically decreases and at all velocities where $w(v)$ is a rational number it branches off hyperbolic and elliptic fixed points of higher period. Due to symmetry reasons they are always created in symmetry related pairs. When the winding numbers of the new elliptical points are rational they also create new periodic points but they cannot be described with the above linearization. Around the origin there are KAM lines and so the bouncing ball orbit and also all the periodic orbits with higher period branching off from it are not accessible to the outside world immediately after their creation. Only for increasing values of v do many of these periodic orbits come into contact with scattering trajectories when the outer layers of the large central KAM island are destroyed (see figure 3(*d*)). At the same time the invariant manifolds of the figure-of-eight orbits undergo various homoclinic and heteroclinic bifurcations (see figures 3(*e*) and 3(*f*)). These are coupled with sequences of saddle-centre bifurcations and cascades of period doublings of the newly created elliptic orbits.

(iv) For increasing values of v the eigenvalues of the figure-of-eight orbits increase to infinity for $v \to v_A$ from below. At the same time the KAM island around the bouncing ball orbit is squeezed flat into a parabolic line. This degenerate case will be described in detail in subsection 4.2. Figure 3(*g*) shows the Poincaré section at a velocity slightly below v_A.

(v) For $v > v_A$ the eigenvalues of the point (0,0) are real again, i.e. the fixed point of the bouncing ball orbit becomes hyperbolic again (figure 3(*h*)). The scattering angle $\theta(b_{loc}, v)$ now is less than π for $b_{loc} > 0$ and so there are no other periodic orbits left except the bouncing ball, which means that the scattering is regular again.

4. The critical velocity $v = v_A$

As we have noted in section 2.1 for $v = v_A$ the scattering angle $\theta(b_{loc}, v)$ is constantly π independent of the impact parameter each time the particle enters one of the Coulomb centres. Therefore the most influential type of periodic orbit at this velocity is a continuum of stadium orbits. Each one of them is represented by a point at $(b, 0)$ in our Poincaré plane with any $b \in [-a, a]$. So our invariant set in the Poincaré plane contains a straight line of fixed points that are all marginally stable: a displacement parallel to the b-axis leads to another fixed point of the same type and a small displacement in direction of the γ-axis causes the trajectory to drift away linearly in time along a line parallel to the b-axis. This is the same behaviour shown by the bouncing ball orbits in billiard systems where parts of the walls are parallel to each other [8]. In the phase space the continuum of stadium orbits forms a two-dimensional parabolic surface S_c.

We also have to keep in mind that although there is a continuum of periodic orbits the particle can only reach the two boundary lines of the parabolic surface (the outermost stadium orbit and its counterrotating symmetry partner) where $b \to a$ and $b \to -a$ when

approaching from outside. This is related to the fact that at the moment of disappearance the homoclinic/heteroclinic intersections of the rest of the invariant set contract to these boundary points of the parabolic surface (see subsection 4.2).

4.1. Time delay statistics

Now we are interested in the number $N(n)$ of particles that are trapped for longer than a given number n of bounces in the Coulomb potentials.

In the (b, γ) plane of incoming asymptotes we define two strips Σ_1, Σ_2 which contain the initial values for all trajectories that reach the two Coulomb centres.

$$\Sigma_1 : -a < b - R\sin\gamma < a \tag{15}$$

$$\Sigma_2 : -a < b + R\sin\gamma < a. \tag{16}$$

All particles starting from Σ_1 hit the centre which is closest to their starting point. They are deflected backwards and disappear again into the asymptotic region after one single bounce. The particles starting from Σ_2 reach the other centre if they are not deflected by the first one. All other initial conditions never reach any of the centres. So the interesting initial conditions for multiple scattering are those which lie in Σ_2 but not in Σ_1.

For each deflection the scattering angle is exactly π and the impact parameter b changes constantly by

$$\Delta b = b' - b = 2R\sin\gamma. \tag{17}$$

For $\gamma > 0$ the impact parameter increases constantly as long as b does not exceed the maximum impact parameter which is given by

$$b_{\max}(\gamma) = a - R\sin\gamma. \tag{18}$$

Therefore the number of bounces for a particle from Σ_2 is given by

$$n(b,\gamma) = \mathrm{trunc}\left(\frac{b_{max} - b}{\Delta b}\right) = \mathrm{trunc}\left(\frac{a-b}{2R\sin\gamma} - \frac{1}{2}\right) \tag{19}$$

where $\mathrm{trunc}(x)$ denotes the integer part of the argument.

It follows that the initial conditions for all particles that reach more than n bounces have to lie below a certain curve if the incident angle γ is positive. For $\gamma < 0$ we get a similar condition which gives us a third strip

$$\Sigma_3(n) : -a < b + (2n+1)R\sin\gamma < a. \tag{20}$$

Note that $\Sigma_3(0) = \Sigma_2$.

Now we can identify all particles which show more than n bounces. They are given by the initial conditions that lie in $\Sigma(n) = \Sigma_3(n) \cap \Sigma_2 \backslash \Sigma_1$ and $N(n)$ is proportional to the area of this region.

In the b–$R\sin\gamma$ plane (figure 4) the boundaries of our strips are straight lines and for $n > 0$, $\Sigma(n)$ consists of two triangles with area

$$A(n) = \frac{a^2}{n(n+1)} \tag{21}$$

and with $N(n)/N(1) = A(n)/A(1)$ we get

$$N(n) = \frac{2N(1)}{n(n+1)}. \tag{22}$$

This means that for large values of n we have a power law decay with $N(n) \sim n^{-\sigma}$ where $\sigma = 2$. As we can see in figure 5 this is in very good agreement with the numerical results.

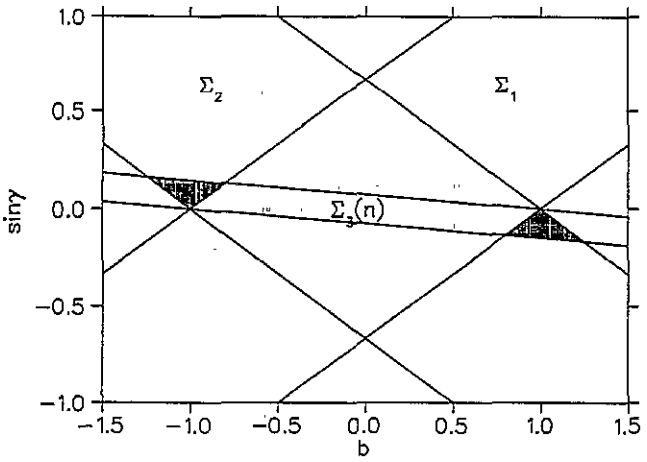

Figure 4. The lines that separate trajectories of different behaviour in the plane of asymptotic initial conditions. The hatched area marks initial conditions leading to more than n bounces. The strip $\Sigma_3(n)$ is plotted for the example of $n = 4$. For more information see section 4.1.

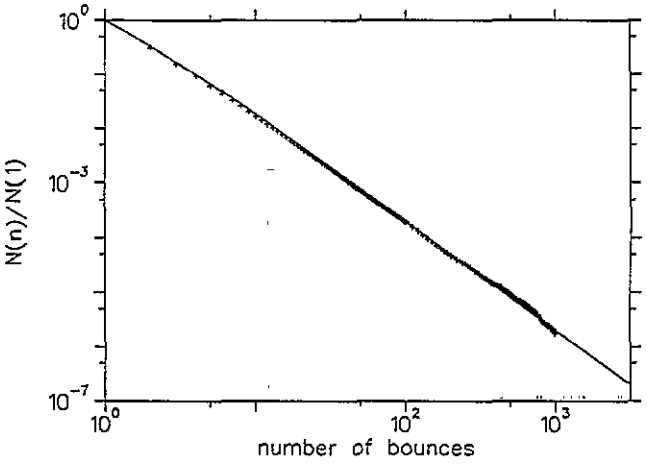

Figure 5. The time delay statistics for $v = v_A$: relative number of trajectories suffering more than n bounces against n in double logarithmic representation. The crosses represent the numerical statistics for randomly chosen initial conditions. The continuous curve corresponds to equation (22).

4.2. Structure of Λ at the critical value

Exactly at $v = v_A$ parts of the figure-of-eight orbits and the droplet orbits run exactly on the cut-off boundary of the potentials. This makes them infinitely unstable, since along the cut-off line the trajectory can go off tangentially at any point. Furthermore the bundle of all other localized orbits except the stadium orbits contract to this cut-off line. The outermost stadium orbit also runs partially on this cut-off line. Therefore there are heteroclinic switches between the figure-of-eight orbits, the droplet orbits and the outermost stadium orbits. Of course, all these localized orbits which run partially on the cut-off line are infinitely unstable. In position space all these unstable orbits are restricted to the following set of finitely many lines: the segments with $|y| < R$ of the tangents to the cut-off lines running parallel to

the y-axis at $x = \pm a$; the segments with $r^2 < R^2 - a^2$ of the tangents to the cut-off lines running through the origin; the segments starting in one centre and touching tangentially the cut-off circle around the other centre; and the upper parts of the cut-off lines themselves which connect and continue the just mentioned tangent segments. In the Poincaré plane all the unstable localized orbits are restricted to the eight points which also belong to either the figure-of-eight orbits or to the outermost stadium orbits or the droplet orbit.

The bundles of invariant manifolds to the unstable localized orbits squeeze together to lines, their scaling factors become zero. This is very similar to the events in an abrupt bifurcation. However, there are also some important differences. First, in our case the eigenvalues of the figure-of-eight shape orbits go to infinity with an algebraic behaviour with power -4 as a function of $d = (v_A^2 - v^2)/(v_A^2 - v_B^2)$ in the Poincaré map. Correspondingly the scaling of the fractal bundle of manifolds of the unstable part of the invariant set follows d^4. This result emerged from the numerical computations and can be derived analytically as follows.

If $v^2 = 1/a - d/R$, then to second order in d the position of the unstable fixed points in the Poincaré map are given by

$$b = 0 \qquad \sin^2\gamma = a^2(1 - d^2(1 - a^2/R^2))/R^2. \tag{23}$$

For the derivative of the deflection function we obtain thereby in lowest order in d the value

$$\frac{d\theta}{db} = 2d^{-2}(R^2 - a^2)^{-1/2}. \tag{24}$$

Taking the linearization of M around this point and calculating its largest eigenvalue μ gives in the leading order in d the result

$$\mu = -4d^{-2}. \tag{25}$$

Since the Poincaré map is M^2, the larger eigenvalue of the figure-of-eight orbit in the Poincaré map is given as μ^2 in leading order in d which explains the power -4. In contrast, in equations (14) and (C6) in [5] it is shown that in a generic abrupt bifurcation the quantity $d\theta/db$ as well as the eigenvalues of periodic points in the symmetry reduced Poincaré map go with $1/d$ per iteration step. At the moment the origin for the difference in the power behaviour of this scaling is not clear to us. It may be connected with our attractive potential wells with hard cut-off, while abrupt bifurcations have been studied so far for repulsive potential mountains only [6].

Second, in our case there is no hyperbolic behaviour of the invariant set directly below v_A in contrast to the generic abrupt bifurcation. This is connected with the behaviour of the bouncing ball orbit and of the KAM island around it for $v \to v_A$. The KAM island around the point (0,0) becomes more and more elongated. Its width in γ direction goes to zero while its width in b direction converges to $2a$. And for $v = v_A$ where $w(v) = 0$ we obtain the continuous line of parabolic fixed points in the Poincaré surface of section.

On intuitive grounds we can understand the collapse of the invariant set to a line as follows. Exactly at $v = v_A$ the scattering angle in each potential hole is exactly π whatever the impact parameter is, as long as $|b| < a$. Therefore the only possible type of localized orbit is the one which is composed of arcs making turns of π inside the potentials and straight line segments parallel to the y-axis in between the potential holes. So the only type of periodic orbits left (except the infinitely unstable ones running exactly on the cut-off line) are the ones of stadium type. All other types of periodic orbits, the ones containing straight line segments not exactly parallel to the y-axis, are lost when $v \to v_A$. In this way the invariant set in the Poincaré map collapses to the subset of points describing perpendicular intersections of the x-axis, i.e. to the line $\sin\gamma = 0$.

The similarities and differences of our scenario at $v = v_A$ with the generic scenarios can be summarized as follows. In the abrupt bifurcation a fully developed chaotic set is created which is hyperbolic in the vicinity of the bifurcation value of the parameter. In our case we have a sudden bifurcation to a partially developed chaotic set. Just below the bifurcation value it is half developed compared to a complete horseshoe of three fixed points. This is also in contrast to the first generic scenario mentioned in the introduction and to the scenario present in this model at $v = v_B$, where the chaotic set starts at development stage zero. In common with a generic abrupt bifurcation the outer periodic orbits of the invariant set become infinitely unstable and the scaling factors of the bundles of invariant manifolds go to zero.

Of course, also the behaviour of the fractal dimension and of the Lyapunov exponent in our case is different from the behaviour in a generic abrupt bifurcation. In our case there exist KAM islands up to the bifurcation value of the parameter. Therefore the partial fractal dimension (fractal dimension of the transversal structure of the bundle of invariant manifolds) always has the value one and the Lyapunov exponent always has the value zero.

5. Symbolic dynamics

Next we describe the approach $v \to v_A$ by a symbolic dynamics. There are three different fixed points in the Poincaré map where the two outer ones belonging to the two figure-of-eight orbits are symmetry related and therefore equivalent. Accordingly the invariant set is a symmetric ternary horseshoe. To describe its development we introduce a formal parameter α in analogy to [9–11]. α gives the development degree of the actual horseshoe compared to a complete ternary horseshoe. The value of α is related to the length of the tendrils of the invariant manifolds of the unstable fixed points. At $v = v_B$ the horseshoe starts at development $\alpha = 0$. For $v \to v_A$ α converges towards $1/2$. The present system has the unusual property that the horseshoe disappears completely at $\alpha = 1/2$ in a sudden bifurcation. It never becomes more than half developed.

In general a symbolic dynamics of an incomplete horseshoe containing KAM lines is of infinite complexity. In the branching tree pruning occurs and we need grammatical rules selecting out the allowed symbol blocks [12–16]. However, as shown in [9], there are intervals of the physical parameter (in our case it is v), for which an approximate symbolic dynamics with finite grammatical rules is valid to a rather high level of the hierarchy. These intervals are the ones in which the tips of the tendrils of low levels of the hierarchy end in gaps of low levels. Then the tips of tendrils of high levels end in the outside region and the tendrils avoid tangencies on low levels which would prevent any possibility even for approximate simple grammatical rules. Each interval of the physical parameter in which such a structure holds belongs to a single value of the formal parameter α. For some more information about the construction of symbolic dynamics for incomplete horseshoes see also [17]. For the sake of brevity we do not repeat here all these ideas, we only apply them to the present system and refer the reader to the references given above.

In this paper we are mainly interested in the degenerate sudden bifurcation at $v = v_A$, $\alpha = 1/2$. To understand the development of the invariant set when the parameters approach this particular value from below, we utilize a sequence of α values which converges to the value $1/2$ from below such that for all values of the sequence we can construct a symbolic dynamics with rather simple rules and which is valid in good approximation to rather high levels of the hierarchy. An appropriate possibility is the sequence $\alpha_k = (3^k - 1)/(2 \cdot 3^k)$ where k runs over positive integers. The cases $k = 1, 2, 3$, $\alpha = 1/3, 4/9, 13/27$ are reached in v intervals lying around $v = 0.9, 0.965, 0.98$ respectively. The corresponding horseshoe

constructions for $k = 1, 2$ are shown in figures 3(*e*) and 3(*f*) respectively.

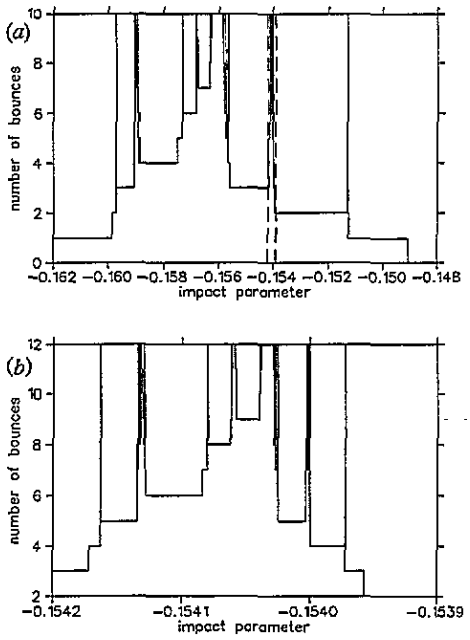

Figure 6. Number n of bounces against the impact parameter b for fixed incoming speed $v = 0.965$ which belongs to the formal parameter value $\alpha = 4/9$. The incoming direction makes an angle of 50 degrees to the y-axis. (*a*) shows the whole structure, (*b*) gives a magnification of the part marked by the two broken lines in (*a*).

As has been explained in [10], the easiest way to construct a symbolic dynamics starts from the scattering function $n(b)$, which is characterized by the number of bounces for fixed incoming direction. In figure 6 we present as an example demonstrating the scattering function for $v = 0.965$, $\alpha = 4/9$. (*a*) gives an overview of the whole structure and (*b*) gives a magnification to show the self-similar regularity of the structure under magnification. Next, on level m we choose the threshold value $n = m$ and find all impact parameter intervals J_j^m in which $n(b) > m$ inside and $n(b) \leqslant m$ outside. In the corresponding branching tree each interval J_j^m is represented by one entry on level m. This is connected with the entry of the interval J_l^{m-1} of level $m-1$ if $J_j^m \subset J_l^{m-1}$. The branching tree corresponding to the scattering function of figure 6 is presented in figure 7. This hierarchy of partly nested intervals coincides with the hierarchical construction of the corresponding homoclinic tangle as shown in figure 3(*f*). In figure 7 the entries are already labelled in the most simple and natural way by the symbols X, Y, Z. These symbol values do not have a one-to-one correspondence to the three fixed points of the Poincaré map.

This type of symbolic dynamics is obtained from a scattering function. Accordingly it only can describe the unstable part of the invariant set which is in contact with the scattering trajectories. It is never able to describe the behaviour inside KAM islands. It also breaks down on the surface of KAM islands. Therefore the symbolic dynamics also breaks down for the scattering behaviour at very high levels of the hierarchy where the tendrils of the invariant manifolds of the figure-of-eight orbits dive into the secondary fractal structures around KAM island. This is the level of hierarchy where in the scattering behaviour non-hyperbolic effects take over and the time delay statistics crosses over from

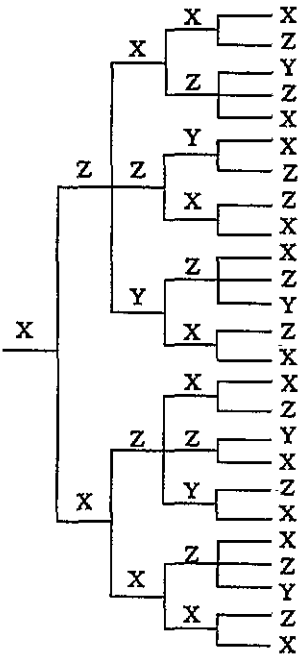

Figure 7. Branching tree corresponding to the scattering function plotted in figure 6. Each entry is labelled by the last digit of its symbolic code.

exponential behaviour to algebraic behaviour [18–20]. For more information on the errors in the approximate symbolic dynamics constructed along this scheme see [9].

If we do the corresponding construction for all parameter values α_k then we obtain the following simple grammatical rules:

(i) On symbol strings ending on X or on Y it is allowed to append X or Z.

(ii) On symbol strings ending on Z but not ending on a string of only Z's of length k it is allowed to append X or Y or Z.

(iii) On symbol strings ending on a block of only Z's of length k it is allowed to append X or Y.

In the limit $k \to \infty$ we obtain the following very simple rules:

(i) On symbol strings ending on X or on Y it is allowed to append X or Z.

(ii) On symbol strings ending on Z it is allowed to append X or Y or Z.

From these rules we obtain the following values for the branching ratio $B_k = B(\alpha_k)$ of the branching tree: $B_1 = 2$, $B_2 \approx 2.27$, $B_3 \approx 2.36$, $B_\infty = 1+2^{1/2}$. The topological entropy of the unstable part of the invariant set is the logarithm of this branching ratio B.

6. Conclusions

It seems rather unusual that our system becomes regular again at small values of the energy. This may be related to the hard cut-off of the potentials. Alternative computations with smooth exponential screening have shown fully developed chaos (a complete horseshoe with three fixed points) for small energy. In addition, in [21] scattering off a smooth two-centre well has been investigated. Here also complicated behaviour has been reported for low energy.

The creation of Λ at $v = v_B$ is a symmetry adapted version of the first generic scenario mentioned in the introduction. Exactly at $v = v_B$ the bouncing orbit C becomes parabolic and branches off the two symmetry-related orbits B. This pitchfork bifurcation is the symmetry adapted counterpart to a saddle-centre bifurcation (see also page 150 in [22]). In this sense the behaviour of Λ at the lower end of its parameter of existence is nothing very unusual. For another instructive example of this route to a chaotic saddle see the collinear model for the HgI_2 molecule presented in [23].

In contrast, the behaviour at the upper end is remarkable. The degenerate sudden disappearance of Λ in this particular model depends essentially on two properties. First on the independence of the deflection angle on the impact parameter for $v = v_A$ and second on the simultaneous loss of the figure-of-eight orbit B which disappears into the cut-off boundary of the potential. This scenario is not stable against deformations of the potential and numerical computations have revealed a rather different and more generic scenario for exponential screening. Moreover it is well known that the two-centre Coulomb potential is completely integrable if there is no cut-off at all.

The occurrence of a single smooth isolated surface of parabolic orbits surrounded by scattering trajectories only is not generic in Hamiltonian scattering systems. On the other hand, parabolic surfaces are also not completely unknown. For example they occur in billiards with walls which are partly running parallel to each other [8]. Such families of periodic orbits can have a profound influence on the quantum behaviour of a system [24, 25]. Parabolic surfaces also occur in hydrodynamic models for scattering chaos, where the parabolic orbits are formed by particles remaining on the wall of an obstacle in the flow [26–27]. However, in these cases the parabolic surface exists independently of the parameter and the structure of the complete invariant set Λ is much more complicated than in our example for $v = v_A$ since in the hydrodynamic models and in the chaotic billiards the smooth parabolic surface is embedded into a complicated chaotic set. Therefore our present example belongs to the simplest class of chaotic scattering systems having a smooth parabolic surface in the phase space which is accessible to scattering trajectories. And its understanding can serve as an initial step prior to the analysis of more complicated invariant sets containing smooth parabolic surfaces as part of more complicated invariant sets.

S_c is an element of marginal stability. In generic Hamiltonian systems the occurrence of subsets of marginal stability is rather common, namely in the form of KAM tori. However, the outermost invariant lines of KAM islands are not smooth and together with their environment of fractal patterns of secondary structures and cantori (for a detailed description see [28]) they lead to a different behaviour of the time delay statistics. Trajectories can find their way out of this fractal cage by a very slow diffusive type of random walk only where the distance travelled grows slower than linearly with time. This process can be described as diffusion in a self-similar Markov tree [29–31]. In contrast near smooth parabolic surfaces the vector field in phase space is parallel to the surface and therefore the distance travelled grows linearly with time for particles initiated nearby. By this mechanism KAM islands lead to the power $\sigma = 1.5$ [18–20] in contrast to $\sigma = 2$ in our present example. In the hydrodynamic examples the power is also $\sigma = 2$ [26, 27]. This allows the following conclusion: if in a Hamiltonian scattering system the scattering trajectories are in contact with a smooth surface of marginal stability only, then this leads to the power $\sigma = 2$ in the time delay statistics in contrast to the rough surface of KAM islands which leads to $\sigma = 1.5$.

Acknowledgments

The authors would like to thank L Benet, N Meyer, T H Seligman and D Trautmann for useful discussions and hints. CJ thanks the Deutsche Forschungsgemeinschaft for a Heisenberg stipendium. This work was partially supported by the Schweizerischer Nationalfonds.

References

[1] 1993 *Chaos* **3** (4)
[2] Bleher S, Grebogi C and Ott E 1989 *Phys. Rev. Lett.* **63** 919
[3] Jung C and Scholz H J 1988 *J. Phys. A: Math. Gen.* **21** 2301
[4] Jung C and Scholz H J 1987 *J. Phys. A: Math. Gen.* **20** 3607
[5] Bleher S, Grebogi C and Ott E 1990 *Physica* D **46** 87
[6] Tel T, Grebogi C and Ott E 1993 *Chaos* **3** 495
[7] Jung C, Mejia-Monasterio C and Seligman T H 1995 *Phys. Lett.* A **198** 306
[8] Berry M V 1981 *Eur. J. Phys.* **2** 91
[9] Rückerl B and Jung C 1994 *J. Phys. A: Math. Gen.* **27** 55
[10] Rückerl B and Jung C 1994 *J. Phys. A: Math. Gen.* **27** 6741
[11] Breymann W and Jung C 1994 *Europhysics Lett.* **25** 509
[12] Cvitanovic P, Gunaratne G and Procaccia I 1988 *Phys. Rev.* A **38** 1503
[13] Auerbach D and Procaccia I 1990 *Phys. Rev.* A **41** 6602
[14] Troll G 1991 *Physica* D **50** 276
[15] Troll G 1992 *Nonlinearity* **5** 1151
[16] Vollmer J and Breymann W 1993 *Helv. Phys. Acta* **66** 91
[17] Davis M J, MacKay R S and Sannami A 1991 *Physica* D **52** 171
[18] Karney C F 1983 *Physica* D **8** 360
[19] Chirikov B and Shepelyansky D L 1984 *Physica* D **13** 395
[20] Hillermeyer C F, Blümel R and Smilansky U 1992 *Phys. Rev.* A **45** 3486
[21] Daniels V, Vallieres M and Yuan J M 1993 *Chaos* **3** 475
[22] Guckenheimer J and Holmes P 1983 *Nonlinear Oscillations, Dynamical Systems, and Bifurcations of Vector Fields* (New York: Springer)
[23] Burghardt I and Gaspard P 1995 *J. Phys. Chem.* **99** 2732
[24] Bai Y, Hose G, Stefanski K and Taylor H S 1985 *Phys. Rev.* A **31** 2821
[25] Vivaldi F, Casati G and Guarneri I 1983 *Phys. Rev. Lett.* **51** 727
[26] Jung C, Tel T and Ziemniak E 1993 *Chaos* **3** 555
[27] Ziemniak E, Jung C and Tel T 1994 *Physica* D **76** 123
[28] Greene J, MacKay R S and Stark J 1986 *Physica* D **21** 267
[29] MacKay R S, Meiss J D and Percival I C 1984 *Physica* D **13** 55
[30] Hanson J D, Cary J R and Meiss J D 1985 *J. Phys. C: Solid State Phys.* **39** 327
[31] Meiss J D and Ott E 1986 *Physica* D **20** 387